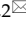Research Paper

In vivo characterization of a novel norepinephrine transporter PET tracer [18F]NS12137 in adult and immature Sprague-Dawley rats

Francisco R. López-Picón[1,2✉*], Anna K. Kirjavainen[3,4*], Sarita Forsback[3,4], Jatta S. Takkinen[1,2], Dan Peters[5,6], Merja Haaparanta-Solin[1,2], and Olof Solin[3,4,7✉]

1. Preclinical Imaging, Turku PET Centre, University of Turku, Turku, Finland
2. Medicity Research Laboratory, University of Turku, Turku, Finland
3. Radiopharmaceutical Chemistry Laboratory, Turku PET Centre, University of Turku, Turku, Finland
4. Department of Chemistry, University of Turku, Turku, Finland
5. DanPET AB, Malmö, Sweden
6. Neurobiology Research Unit, Copenhagen University Hospital, Rigshospitalet, Copenhagen, Denmark
7. Accelerator Laboratory, Åbo Akademi University, Turku, Finland

*The authors contributed equally to this work

✉ Corresponding author: Francisco R. López-Picón, PhD, PET Preclinical Imaging, Medicity Research Laboratory, Turku PET Centre, Tykistökatu 6A, 4th floor, FI-20520 Turku, Finland. E-mail: francisco.lopez@utu.fi. Tel. +358-2-333-7019

Abstract

Norepinephrine modulates cognitive processes such as working and episodic memory. Pathological changes in norepinephrine and norepinephrine transporter (NET) function and degeneration of the locus coeruleus produce irreversible impairments within the whole norepinephrine system, disrupting cognitive processes. Monitoring these changes could enhance diagnostic accuracy and support development of novel therapeutic components for several neurodegenerative diseases. Thus, we aimed to develop a straightforward nucleophilic fluorination method with high molar activity for the novel NET radiotracer [18F]NS12137 and to demonstrate the ability of [18F]NS12137 to quantify changes in NET expression.

Methods: We applied an 18F-radiolabeling method in which a brominated precursor was debrominated by nucleophilic 18F-fluorination in dimethyl sulfoxide. Radiolabeling was followed by a deprotection step, purification, and formulation of the radiotracer. The [18F]NS12137 brain uptake and distribution were studied with *in vivo* PET/CT and *ex vivo* autoradiography using both adult and immature Sprague-Dawley rats because postnatal NET expression peaks at 10–20 days post birth. The NET specificity for the tracer was demonstrated by pretreatment of the animals with nisoxetine, which is well-known to have a high affinity for NET.

Results: [18F]NS12137 was successfully synthesized with radiochemical yields of 18.6±5.6%, radiochemical purity of >99%, and molar activity of >500 GBq/µmol at the end of synthesis. The *in vivo* [18F]NS12137 uptake showed peak standard uptake values (SUV) of over 1.5 (adult) and 2.2 (immature) in the different brain regions. Peak SUV/30 min and peak SUV/60 min ratios were calculated for the different brain regions of the adult and immature rats, with a peak SUV/60 min ratio of more than 4.5 in the striatum of adult rats. As expected, *in vivo* studies demonstrated uptake of the tracer in brain areas rich in NET, particularly thalamus, neocortex, and striatum, and remarkably also in the locus coeruleus, a quite small volume for imaging with PET. The uptake was significantly higher in immature rats compared to the adult animals. *Ex vivo* studies using autoradiography showed very strong specific binding in NET-rich areas such as the locus coeruleus and the bed nucleus of the stria terminalis, and high binding in larger grey matter areas such as the neocortex and striatum. The uptake of [18F]NS12137 was dramatically reduced both *in vivo* and *ex vivo* by pretreatment with nisoxetine, demonstrating the specificity of binding.

Conclusions: [18F]NS12137 was synthesized in good yield and high molar activity and demonstrated the characteristics of a good radiotracer, such as good brain penetration, fast washout, and high specific binding to NET.

Introduction

Norepinephrine (NE) modulates cognitive processes such as working and episodic memory. Changes in NE, norepinephrine transporter (NET), and degeneration in the locus coeruleus (LC) produce impairment in the LC-NE system, disrupting cognitive processes [1]. LC-NE system dysregulation contributes to a wide array of non-cognitive symptoms of dementia such as agitation and aggression [2-5].

The LC is the first human brain region where Alzheimer's disease (AD) pathology emerges [6,7]. In addition, studies with transgenic animal models of AD where the LC has been lesioned using the selective neurotoxin *N*-(2-chloroethyl)-*N*-ethyl-2-bromobenzylamine hydrochloride (i.e., DSP-4) have shown aggravation of tau and amyloid pathology and increased neuroinflammation and cognitive decline [8-10]. Recent research suggests the importance of preserving the LC-NE nuclei to prevent cognitive decline in aging [11]. Post-mortem AD brain analyses have shown 50% cell loss in the LC and a 30% reduction in cortical NE levels [12].

Several [11]C- and ^{18}F-labeled analogues of the antidepressant reboxetine have been introduced as NET radiotracers for monitoring NET *in vivo* using positron emission tomography (PET). Some of these tracers include [18F]fluororeboxetine, [11C]methylreboxetine [13-16], and [18F]fluoromethylreboxetine [13,17-19]. In addition, [11C]nisoxetine [13,20,21] and its analog [11C]thionisoxetine [22] have been used as NET radiotracers in small animal studies. NET-selective reuptake inhibitors such as [11C]lortalamine, [11C]oxaprotiline [13,21], [11C]talsupram, [11C]talopram [18,19,22,23], [11C]desipramine, and hydroxy-[11C]desipramine [22,24] have also been evaluated as possible NET tracers.

Although numerous NET-selective radiotracers have been introduced for brain imaging, few have emerged for clinical use. The above candidates have suitable NET binding affinities and lipophilicities but also show significant non-specific binding in the brain, which is not desirable for a good diagnostic ratiotracer. The reboxetine analogue (*S*,*S*)-[18F]FMeNER-D$_2$ [17-19], however, can quantify NET density in human cerebral cortex despite non-optimal kinetics and disturbing defluorination.

Previously, we developed the electrophilic fluorination of *exo*-3-[(6-[18F]fluoro-2-pyridyl)oxy]-8-azabicyclo[3.2.1]-octane, [18F]NS12137 [25,26], a fluorinated analogue of [11C]NS8880 [27] that showed higher binding affinity for NET (K_i ~9.5 nM) than for serotonin transporters (K_i ~550 nM) and dopamine transporters (K_i ~650 nM) (Material S1) [28]. In the current study, we aimed to develop the nucleophilic fluorination of [18F]NS12137 and characterize it by *in vivo* PET and *ex vivo* autoradiography (ARG). In the current study we used mature and immature rats to demonstrate the ability to quantitate different levels of NET expression. The NET density peaks in the rat brain at 10-20 days of age, and in the LC, is approximately seven-fold higher than in the LC of adult rats [29]. Here, we demonstrate the applicability of [18F]NS12137 PET imaging to quantify and monitor the NET and LC-NE systems, which has the potential to enhance diagnosis and treatment strategies for psychiatric and neurodegenerative diseases.

## Methods

Radiosynthesis and formulation of [18F]NS12137

The precursor(*exo-tert*-butyl-3-[(6-bromo-2-pyridyl)oxy]-8-azabicyclo[3.2.1]-octane-8-carboxylate, **1**) and reference for NS12137 (*exo*-3-[(6-fluoro-2-pyridyl)oxy]-8-azabicyclo[3.2.1]-octane, **3**) were obtained from DanPET AB, Malmö, Sweden, and NeuroSearch A/S, Ballerup, Denmark. All other reagents and solvents were obtained from commercial suppliers and used without further purification.

[18F]Fluoride was produced with the nuclear reaction, $^{18}O(p,n)^{18}F$, by irradiating ^{18}O-enriched water (^{18}O, >98 atom%, Rotem Industries, Israel) with an 18 MeV proton beam, produced with a CC-18/9 cyclotron (Efremov Scientific Research Institute of Electrophysical Apparatus, St Petersburg, Russia). Briefly, a niobium target was filled with ^{18}O-enriched water (2.1 mL) for irradiation. At the end of bombardment (EOB), the produced ^{18}F-fluoride was isolated from the target water at room temperature (RT) on an anion exchange cartridge (QMA, Waters Corporation, Milford, MA, USA). The initial amount of [18F]F- used in the syntheses was 7.5±2.9 GBq (n=4).

The brominated precursor **1** (3.6-5.8 mg, 9.4-15.3 μmol), dissolved in dimethyl sulfoxide (DMSO, 1.0

mL), was added into the reaction vessel containing a dry $^{18}F^-/K_2CO_3/K222$ complex. The reaction solution was heated at 185 °C for 15 min (**Figure 1**). The reaction mixture was cooled down for 2 min and then diluted with water (30 mL) and this mixture was loaded onto a preconditioned (7 mL EtOH and 10 mL water) light tC18 SPE cartridge (Waters Corp., Milford MA, USA). The cartridge was then flushed with air (60 mL). The *tert*-butoxy-protected intermediate [^{18}F]**2** (**Figure 1**) was released from the SPE cartridge with tetrahydrofuran (THF, 700 µL). THF was evaporated to dryness with helium flow at RT. Subsequently, HBr (48%, 150 µL) was added on the residual and the solution was heated at RT for 5 min to remove the protective Boc-group by acidic hydrolysis. After hydrolysis the crude intermediate solution was

diluted with semi-preparative HPLC eluent (1.8 mL) and purified using the semi-preparative HPLC method (HPLC method 1) described below. The purified [^{18}F]NS12137 ([^{18}F]**3)** fraction was collected, diluted with water (20 mL). The diluted product fraction was loaded onto the preconditioned Plus C18 SPE cartridge (Waters Corp., Milford MA, USA). The loaded SPE cartridge was rinsed with water (20 mL) to remove HPLC eluent. [^{18}F]**3** was released from the cartridge and formulated for preclinical studies with EtOH (0.8 mL) and 0.9% NaCl-solution (5 mL). The chemical and radiochemical purity of the [^{18}F]**2** was analyzed using HPLC method 2, and the [^{18}F]**3** was analyzed using HPLC method 3, described below (**Figure 2**).
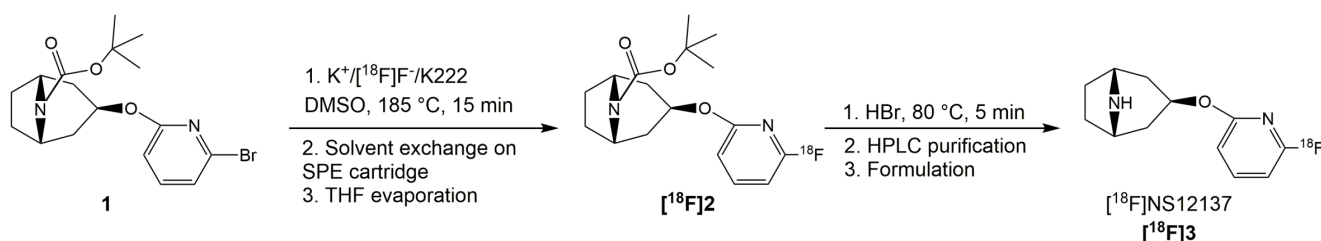
Figure 1. Radiosynthetic route of [^{18}F]NS12137 ([^{18}F]**3**).
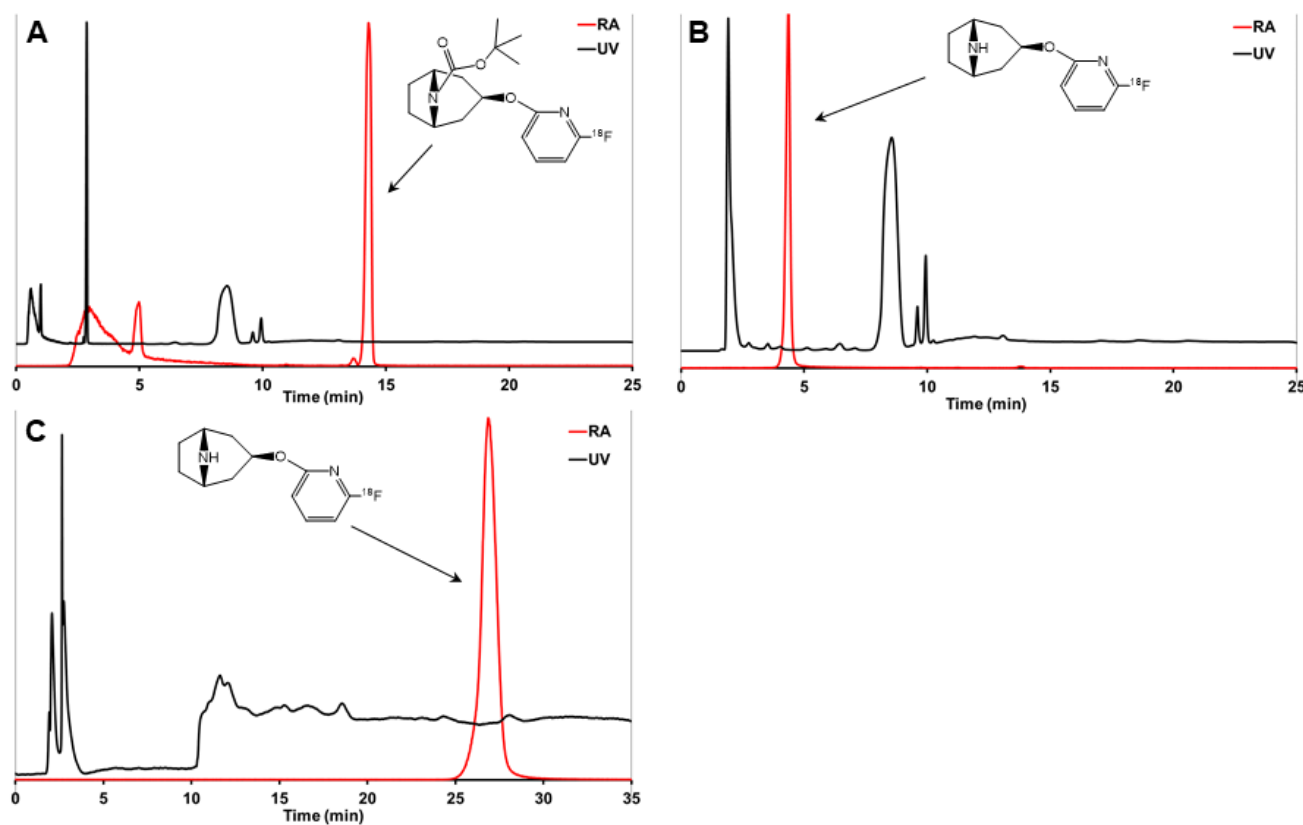
Figure 2. Analytical HPLC chromatograms of crude reaction mixture before deprotection **(A)**, [^{18}F]**3** after deprotection **(B)**, and the final purified product [^{18}F]**3** **(C)**. [^{18}F]**2** is (A) and [^{18}F]**3** is (B) were analyzed using analytical HPLC method 2 and [^{18}F]**3** in (C) was analyzed using analytical HPLC method 3.

The semi-preparative radio-HPLC (HPLC method 1) was used to purify the [18F]**3**. A Jasco PU-2089 Plus (JASCO Europe s.r.l., Cremella, Italy) preparative HPLC pump connected to a Gemini C18 column (5 µm, 10×250 mm, Phenomenex, Milford, MA, USA) was used for the separation. The column was eluted with 7 mM KH_2PO_4 (A) and CH_3CN (B) gradient at a flow rate of 5.0 mL/min. The column was eluted first for 5 min with 100% A, and the content of B was increased to 8% at 5.1 min. The column was eluted for 5.1-41 min with 92% A and 8% B at 5.1 min. After 41 min, the content of B was increased to 80% to wash the column until 60 min.

The analytical radio-HPLC (HPLC methods 2 and 3) was performed with a VWR-Hitachi L-2130 HPLC pump (VWR Hitachi, VWR International GmbH, Darmstadt, Germany) equipped with a VWR-Hitachi L-2400 UV-absorption detector (λ=230 nm), a 2×2-inch NaI crystal for detecting radioactivity, and a Gemini C18 column (5 µm, 4.6×250 mm, Phenomenex, Milford, MA, USA). The analytical HPLC column was eluted with 7 mM KH_2PO_4 (A) and CH_3CN (B) gradient at a flow rate of 1.5 mL/min. HPLC method 2 was used to analyze the protected intermediate [18F]**2** (**Figure 2**). The C18 column was eluted for the first 5 min with 20% B that was then increased to 80% over the next 5 min, and the column was eluted with 80% B for 25 min. The HPLC method 3 was used to analyze [18F]**3** (**Figure 2**), in which the column was eluted for the first 5 min with 100% A and the content of B increased to 8% at 5.1 min.

Animals

All animal experiments were approved by the Regional State Administrative Agency for Southern Finland (ESAVI/3899/04.10.07/2013 and ESAVI/4499/04.10.07/2016). Adult male Sprague-Dawley rats ages 2-3 months (n=3; 287.0±5.2 g) and immature male Sprague-Dawley rats ages 14-16 days (n=9; 44.5±4.6 g) were used. All animals were group-housed under standard conditions (temperature 21±3 °C, humidity 55±15%, lights on from 6:00 a.m. until 6:00 p.m.) and had *ad libitum* standard food access and tap water.

In vivo PET imaging

Rats were anesthetized with a 2.5% isoflurane/oxygen mixture 30 min prior to injection and then injected intravenously with [18F]**3** (adults: 38.5±1 MBq; immature: 10.2±2.5 MBq) for scanning with an Inveon Multimodality PET/computed tomography (CT) scanner (Siemens Medical Solutions, Knoxville, TN, USA). A few drops of Oftagel (2.5 mg/g; Santen, Tampere, Finland) were applied to the eyes of the animals to prevent eye

dryness. The scanner has an axial 12.7 cm field of view, and 10 cm transaxial field of view generating images from 159 transaxial slices. Rats were scanned for 10 min with CT for attenuation correction and anatomical reference, and immediately after that, the tracer was injected and a 60 min dynamic PET scan started in tandem.

The specificity studies of [18F]**3** were performed using the NET-selective compound nisoxetine (5 mg/kg; RBI, Natick, MA, USA). Nisoxetine was administered intraperitoneally in isotonic saline 30 min prior to injection of [18F]**3** to adult (n=3) and immature (n=3) rats.

Ex vivo studies

For the *ex vivo* studies, the rats used for *in vivo* studies were sacrificed immediately after the 60 min PET scan. The brain was dissected and weighed, and the radioactivity was measured with a gamma counter (Wizard2 3″, PerkinElmer, Turku, Finland). The brain was then quickly frozen in isopentane (2-methylbutane; Sigma-Aldrich) on dry ice. Coronal brain sections of 20 µm were obtained using a cryostat (Leica CM3050S, Germany). The sections were mounted on a glass slide (Superfrost Ultra Plus, Thermo Fisher, USA). The slides were exposed to an image plate (Fuji BAS Imaging Plate TR2025, Fuji Photo Film Co., Ltd., Tokyo, Japan) for about two half-lives of the radioisotope in question.

After the exposure, the imaging plates were scanned with BAS-5000 reader (Fuji, Japan) with a resolution of 25 µm, and the saved images on the computer were analyzed by AIDA Image Analyzer 4.5 software (Raytest, Isotopenmessgeräte, Straubenhardt, Germany). The regions of interest were drawn on the LC, bed nucleus of the stria terminalis (BNST), neocortex (CTX), striatum (STR), and cerebellum (CB). The regions of interest (ROIs) were analyzed as photostimulated intensity/area (PSL/mm^2) and presented as ratios relative to the CB. LC and BNST, CTX, and STR ratios to CB ratios were calculated in the adult and immature rats from the ARGs.

Analysis of PET data

For image analysis, dynamic PET images were first co-registered with the corresponding CT image for a robust anatomical alignment and then with an averaged RAT MRI template for a rigid registration for the adjustment of standardized volumes of interest. Volumes of interest were placed in the whole brain, CTX, thalamus, STR, and CB with Inveon Research Workplace 3.0 (Siemens Medical Solutions). The [18F]**3** *in vivo* uptake was quantified as standardized uptake value (SUV).

Statistics

The results are reported as group mean average ± standard deviation (SD). All statistical analyses were performed with GraphPad Prism (GraphPad Software, v. 5.01, San Diego, CA, USA). Differences between the non-blocked and nisoxetine-blocked groups were analyzed using unpaired t-tests. Differences were considered statistically significant if two-tailed $p<0.05$.

Results

Synthesis of [¹⁸F]3

The total synthesis time was 133 ± 14 min and the decay-corrected radiochemical yield of [¹⁸F]**3** was 18.6 ± 5.9% (n = 4) calculated from the initial ¹⁸F-activity at EOB and the amount of [¹⁸F]**3** after purification and formulation. The radiochemical purity was >99%, and the molar activity (A_m) of the tracer was high (>500 GBq/µmol).

In vivo [¹⁸F]3 uptake in adult and immature rat brain

The brain uptake of [¹⁸F]**3** was studied in adult and immature Sprague-Dawley rats using *in vivo* PET imaging. **Table 1** shows the average peak uptake (as SUV), peak/30 min, and peak/60 min ratio in adult and immature rats in the whole brain and CTX. The peak uptake of [¹⁸F]**3** was reached at 4 min after injection in immature and adult rats. The peak uptake in immature rats is higher than in the adults in whole brain (2.28 vs. 1.57), CTX (2.23 vs. 1.61), thalamus (2.82 vs. 2.09), and STR (2.46 vs. 1.82). The peak/30 min and the peak/60 min ratios show the rapid clearance of [¹⁸F]**3** in high and low NET-containing brain areas.

The initial *in vivo* brain uptake of [¹⁸F]**3** in adult and immature rats showed binding in all NET-containing brain areas with high binding in the CTX, thalamus, and the LC between 0 to 20 min summed frames (**Figure 3A-B**). After the washout, between 50- to 60-min summed frames, the signal in the brain of the adult rats decreased, and accumulation in the skull was observed. In the immature rats, brain signal was still detected, especially in the LC and skull (**Figure 3C-D**).

The specificity of [¹⁸F]**3** was tested *in vivo* by injecting a moderate dose of nisoxetine. **Figure 4** shows SUV time activity curves (TACs) from immature rat whole brain, CTX, thalamus, and STR for untreated and nisoxetine treated rats. The uptake of [¹⁸F]**3** in nisoxetine treated rat was significantly reduced.

Ex vivo [¹⁸F]3 uptake in adult and immature rat brain

In the adult rats (**Figure 5A**), binding was detected in all NET-containing areas, with high binding in LC, BNST, and thalamus and with low binding in the CB. The blocking of [¹⁸F]**3** uptake with nisoxetine (5 mg/kg) abolished the binding in LC and BNST. In the immature rats (**Figure 5B**), similar brain binding of [¹⁸F]**3** was detected, including a higher binding in the BNST and LC and the reduction of binding by pre-treatment with nisoxetine.

The quantification of the ARG images as ratios of different areas to the CB showed that the highest ratios were obtained in the LC (8.8±1.3; 4.9±1.4) and BNST (2.5±0.1; 3.6±0.4) of immature and adult rats, respectively. The CTX (1.5±0.2; 1.7±0.1) and STR (1.3±0.1; 2.3±0.1) ratios were more modest (**Figure 5C**).

Table 1. SUVs at peak uptake, 30 min, and 60 min after injection, and peak/30 min and peak/60 min ratios in adult (2-3 months old, n=3) and immature (14-16 days old, n=6) rats in the whole brain, neocortex, thalamus, striatum and cerebellum.

Adult rats	Peak (SUV)	30 min after injection (SUV)	60 min after injection (SUV)	Ratio peak/30 min	Ratio peak/60 min
Brain	1.57	0.83	0.61	1.90	2.56
Neocortex	1.61	0.91	0.63	1.77	2.56
Thalamus	2.09	0.77	0.38	2.69	5.50
Striatum	1.82	0.83	0.40	2.19	4.54
Cerebellum	1.69	0.8	0.82	2.11	2.05
Immature rats	Peak (SUV)	30 min after injection (SUV)	60 min after injection (SUV)	Ratio peak/30 min	Ratio peak/60 min
Brain	2.28	1.36	0.84	1.69	2.72
Neocortex	2.23	1.44	0.89	1.55	2.50
Thalamus	2.82	1.47	0.85	1.92	3.33
Striatum	2.46	1.44	0.84	1.70	2.92
Cerebellum	2.23	1.12	0.65	1.99	3.38
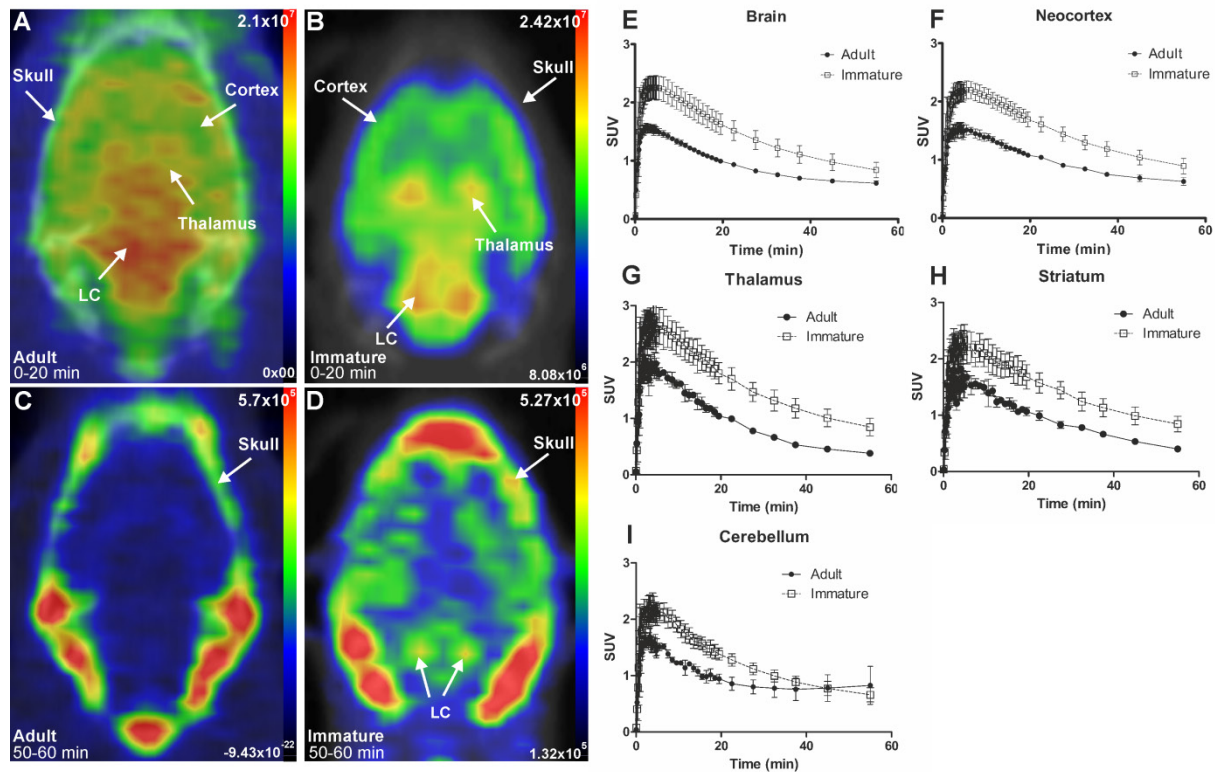
Figure 3. Representative *in vivo* summed PET images of [18F]NS12137 uptake in adult (left) and immature (right) Sprague-Dawley rats 0-20 min **(A-B)** and 50-60 min **(C-D)** after injection. **(E-I)** Average time activity curves (TACs) of [18F]NS12137 uptake in the whole brain, neocortex, thalamus, striatum, and cerebellum in adult (n=3) and immature rats (n=6). Values in the graphs are presented as mean ± SD.
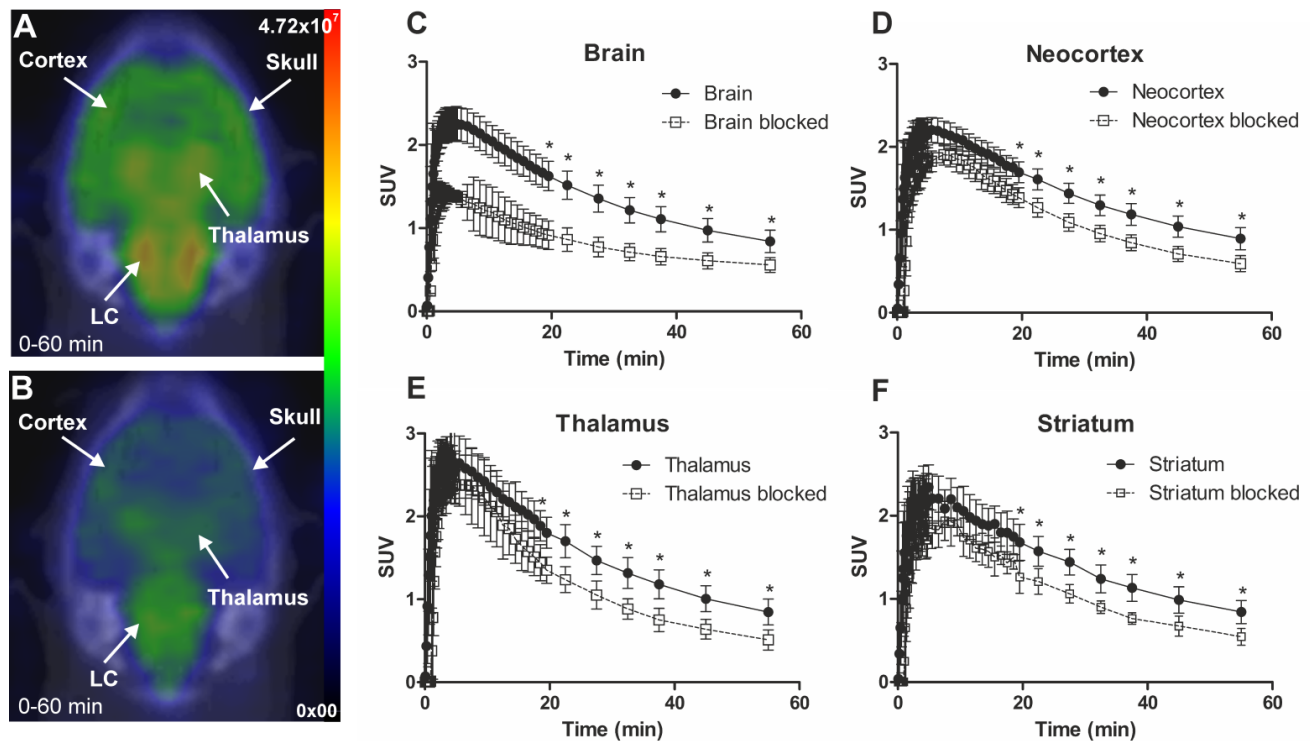
Figure 4. Representative *in vivo* summed (0-60 min) PET images of [18F]NS12137 uptake in immature Sprague-Dawley rats unblocked **(A)** and blocked with 5 mg/kg of nisoxetine **(B)**. Average time activity curves (TACs) of [18F]NS12137 uptake in the whole brain, neocortex, thalamus, and striatum in unblocked (n=6) and blocked (n=3) immature rats **(C-F)**. Values in the graphs are presented as mean ± SD.
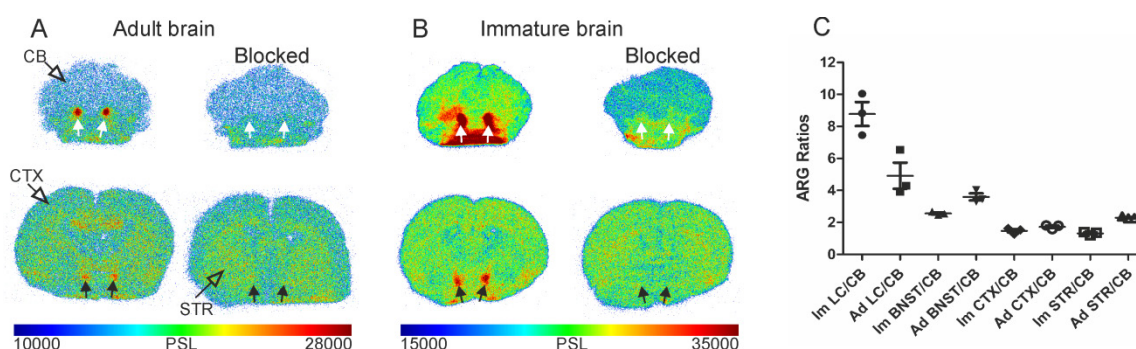
Figure 5. Representative *ex vivo* autoradiographic images (ARG) of brains from unblocked and blocked with 5 mg/kg nisoxetine adult **(A)** and immature **(B)** Sprague-Dawley rats 60 min after [^{18}F]NS12137 injection at the level of the locus coeruleus (LC) and bed nucleus of the stria terminalis (BNST). White arrows indicate the location of the LC and black arrows indicate the location of BNST. **(C)** LC, BNST, neocortex (CTX), and striatum (STR) to cerebellum (CB) ratios calculated from the adult (Ad) and immature (Im) ARG brain image values (mean ± standard deviation).

Discussion

In the present study, we developed the nucleophilic fluorination of the novel ^{18}F-labeled NET tracer [^{18}F]**3**, with high A_m, and performed *in vivo* and *ex vivo* evaluations in adult and immature rats. The immature rats were included in the study because brain NET expression peaks in early postnatal development (5-20 days) and later declines to lower levels in adulthood [29]. In the previous study, we developed an electrophilic fluorination of [^{18}F]**3**, which had an A_m close to 9 GBq/µmol [25]. In the current study, with the development of the nucleophilic fluorination, the A_m was greatly increased, up to >500 GBq/µmol.

Good brain uptake and rapid clearance are desirable characteristics for a suitable radiotracer to achieve a high signal-to-noise ratio in the shortest possible PET scan time. Our current tracer has a high initial uptake and a very good clearance as shown by the high peak/30 min and peak/60 min ratios (**Table 1** and **Figure 3**). In contrast, previous PET studies with non-human primates and humans using (S,S)-[^{18}F]-FMeNER-D$_2$ showed slower clearance and needed scans of up to 240 min to reach similar ratios to the ones obtained in the current study [16,30]. Although, it is difficult to translate the results from rodents to humans due to typically faster kinetics in rodents as compared to humans. Our upcoming human studies with [^{18}F]**3** will show if we are able to achieve higher specific signals at earlier time points than those achieved with previous NET radiotracers. This would then allow shorter dynamic scans and better quantification of not only those areas with high concentration of NET, but also those areas with lower levels of NET that are thus more sensitive to slow tracer clearance.

Our *in vivo* PET experiments allowed us to detect highly expressed NETs in the LC of immature rats because [^{18}F]**3** shows high specific binding and fast clearance. Our *ex vivo* experiments confirmed the *in vivo* results; and, with the better spatial resolution, we could quantify even small NET-rich areas, such as LC and BNST. Although the size of the LC in rats is smaller than 1 mm^3, in humans, the LC reconstruction by German et al. showed a rostrocaudal extent of approximately 16 mm and unilateral areas from 32.8 to 17.6 mm^2 in the youngest to oldest brains [31]. A more recent study showed that the LC volume varied from 5.8 to 21.7 mm^3 (mean: 12.8 mm^3) with no significant sex differences [32]. This difference in size between the rats and humans and the positive ability of imaging rat LC suggest the possibility of quantifying [^{18}F]**3** uptake in human LC and the follow-up of LC integrity.

The possible *in vivo* quantification of NET in different brain areas, including small NET-rich brain areas such as the LC and the BNST in humans, is an emerging interest. Monitoring NET changes in the LC could be useful to monitor cell integrity and for early detection of AD even before onset of cognitive decline. The NET-rich area BNST is a cluster of nuclei surrounding the caudal part of the anterior commissure and is attracting interest because of its involvement in neuropsychiatric disorders and addiction [33,34]. The detection of BNST in the current study suggests the possibility of NET quantification in human BNST using [^{18}F]**3** to further assess the role of NE in neuropsychiatric disorders, such as anxiety.

In the present study, we observed defluorination of [^{18}F]**3** with subsequent ^{18}F-uptake in the skull, as seen in the 50-60 min summed PET images (**Figure 3**). The accumulation of ^{18}F-fluoride in the adult rat skull stemming from the defluorination of [^{18}F]**3** was described in our previous publication [25]. In the current study, the spillover caused by the defluorination does not appear to substantially affect the tracer uptake quantification in the neocortex, striatum or thalamus as observed in the TACs of **Figure 3**, while a clear influence is observed in the

adult rat cerebellum. In any case, species differences have been identified in defluorination between rodents and humans for tracers such as translocator protein radiotracer [18F]PBR06 [35] and metabotropic glutamate receptor 5 radiotracer [18F]SP203 [36]; in some cases, the defluorination has been greatly diminished with pharmacological treatments, as with the cytochrome P450 2E1 inhibitor miconazole and the 5-HT$_{1A}$ receptor radioligand [18F]FCWAY [37]. In upcoming first-in-human studies, the defluorination [18F]**3** will be monitored, and the possible influence on the signal quantification will be evaluated.

Conclusions

The novel NET tracer [18F]NS12137 can be produced in good yield and with high molar activity. [18F]NS12137 shows superior combined characteristics than existing NET tracers, such as good brain penetration, fast clearance, and high NET specificity in adult and immature rats.

Abbreviations

A$_m$: molar activity; ARG: autoradiography; BNST: bed nucleus of the stria terminalis; CB: cerebellum; CH$_3$CN: acetonitrile; CT: computed tomography; CTX: neocortex; DSP-4: *N*-(2-chloroethyl)-*N*-ethyl-2-bromobenzylamine hydrochloride; DMSO; dimethyl sulfoxide; EOB: end of bombardment; FOV: field of view; GBq: gigabecquerel; HPLC: high-performance liquid chromatography; K222: 4,7,13,16,21,24-Hexaoxa-1,10-diazabicyclo[8.8.8]hexacosane; LC: locus coeruleus; MBq: megabecquerel; MRI: magnetic resonance imaging; NE: norepinephrine; NET: norepinephrine transporter; [18F]NS12137: *exo*-3-[(6-[18F]fluoro-2-pyridyl)oxy]-8-azabicyclo[3.2.1]-octane; [18F]**3**: [18F]NS12137; PET: positron emission tomography; RT: room temperature; SD: standard deviation; SPE: solid phase extraction; STR: striatum; SUV: standardized uptake value; TAC: time activity curve.

Acknowledgments

Competing Interests

Authors, Francisco R. López-Picón, Anna K. Kirjavainen, Sarita Forsback, Jatta S. Takkinen, Merja Haaparanta-Solin, and Olof Solin declare that they do not have competing interests.

DanPET AB (100% owned by Dan Peters, CEO) is the registered owner of the US patent US7407970 covering the chemical structure of NS12137.

References

1. Zarow C, Lyness SA, Mortimer JA, Chui HC. Neuronal loss is greater in the locus coeruleus than nucleus basalis and substantia nigra in Alzheimer and Parkinson diseases. Arch Neurol. 2003; 60: 337-341.
2. Lyketsos CG, Lopez O, Jones B, Fitzpatrick AL, Breitner J, DeKosky S. Prevalence of neuropsychiatric symptoms in dementia and mild cognitive impairment: results from the cardiovascular health study. JAMA. 2002; 288: 1475-1483.
3. Finkel SI. Behavioral and psychological symptoms of dementia: a current focus for clinicians, researchers, and caregivers. J Clin Psychiatry. 2001; 62 Suppl 21:3-6.
4. Mega MS, Cummings JL, Fiorello T, Gornbein J. The spectrum of behavioral changes in Alzheimer's disease. Neurology. 1996; 46: 130-135.
5. Sink KM, Covinsky KE, Newcomer R, Yaffe K. Ethnic differences in the prevalence and pattern of dementia-related behaviors. J Am Geriatr Soc. 2004; 52: 1277-1283.
6. Braak H, Del Trecidi K. Neuroanatomy and pathology of sporadic Alzheimer's disease. Adv Anat Embryol Cell Biol. 2015; 215: 1-162.
7. Mravec B, Lejavova K, Cubinkova V. Locus (coeruleus) minoris resistentiae in pathogenesis of Alzheimer's disease. Curr Alzheimer Res. 2014; 11: 992-1001.
8. Heneka MT, Ramanathan M, Jacobs AH, et al. Locus ceruleus degeneration promotes Alzheimer pathogenesis in amyloid precursor protein 23 transgenic mice. J Neurosci. 2006; 26: 1343-1354.
9. Rey NL, Jardanhazi-Kurutz D, Terwel D, et al. Locus coeruleus degeneration exacerbates olfactory deficits in APP/PS1 transgenic mice. Neurobiol Aging. 2012;33:426.e421-411.
10. Chalermpalanupap T, Schroeder JP, Rorabaugh JM, et al. Locus coeruleus ablation exacerbates cognitive deficits, neuropathology, and lethality in P301S tau transgenic mice. J Neurosci. 2018; 38: 74-92.
11. Wilson RS, Nag S, Boyle PA, et al. Neural reserve, neuronal density in the locus ceruleus, and cognitive decline. Neurology. 2013; 80: 1202-1208.
12. Matthews KL, Chen CP, Esiri MM, Keene J, Minger SL, Francis PT. Noradrenergic changes, aggressive behavior, and cognition in patients with dementia. Biol Psychiatry. 2002; 51: 407-416.
13. Ding YS, Lin KS, Logan J, Benveniste H, Carter P. Comparative evaluation of positron emission tomography radiotracers for imaging the norepinephrine transporter: (*S*,*S*) and (*R*,*R*) enantiomers of reboxetine analogs ([11C]methylreboxetine, 3-Cl-[11C]methylreboxetine and [18F]fluororeboxetine), (*R*)-[11C]nisoxetine, [11C]oxaprotiline and [11C]lortalamine. J Neurochem. 2005; 94: 337-351.
14. Ding YS, Lin KS, Logan J. PET imaging of norepinephrine transporters. Curr Pharm Des. 2006; 12: 3831-3845.
15. Gallezot JD, Weinzimmer D, Nabulsi N, et al. Evaluation of [(11)C]MRB for assessment of occupancy of norepinephrine transporters: Studies with atomoxetine in non-human primates. Neuroimage. 2011; 56: 268-279.
16. Schou M, Halldin C, Sovago J, et al. PET evaluation of novel radiofluorinated reboxetine analogs as norepinephrine transporter probes in the monkey brain. Synapse. 2004; 53: 57-67.
17. Schou M, Halldin C, Pike VW, et al. Post-mortem human brain autoradiography of the norepinephrine transporter using (*S*,*S*)-[18F]FMeNER-D$_2$. Eur Neuropsychopharmacol. 2005; 15: 517-520.
18. Seneca N, Gulyas B, Varrone A, et al. Atomoxetine occupies the norepinephrine transporter in a dose-dependent fashion: a PET study in nonhuman primate brain using (*S*,*S*)-[18F]FMeNER-D$_2$. Psychopharmacology (Berl). 2006; 188: 119-127.
19. Zeng F, Mun J, Jarkas N, et al. Synthesis, radiosynthesis, and biological evaluation of carbon-11 and fluorine-18 labeled reboxetine analogues: potential positron emission tomography radioligands for *in vivo* imaging of the norepinephrine transporter. J Med Chem. 2009; 52: 62-73.
20. Haka MS, Kilbourn MR. Synthesis and regional mouse brain distribution of [11C]nisoxetine, a norepinephrine uptake inhibitor. Int J Rad Appl Instrum B. 1989; 16: 771-774.
21. Lin KS, Ding YS. Synthesis and C-11 labeling of three potent norepinephrine transporter selective ligands ((*R*)-nisoxetine, lortalamine, and oxaprotiline) for comparative PET studies in baboons. Bioorg Med Chem. 2005; 13: 4658-4666.
22. Schou M, Sovago J, Pike VW, et al. Synthesis and positron emission tomography evaluation of three norepinephrine transporter radioligands: [C-11]desipramine, [C-11]talopram and [C-11]talsupram. Mol Imaging Biol. 2006; 8: 1-8.

23. McConathy J, Owens MJ, Kilts CD, et al. Synthesis and biological evaluation of [¹¹C]talopram and [¹¹C]talsupram: candidate PET ligands for the norepinephrine transporter. Nucl Med Biol. 2004; 31: 705-718.

24. Van Dort ME, Kim JH, Tluczek L, Wieland DM. Synthesis of ¹¹C-labeled desipramine and its metabolite 2-hydroxydesipramine: potential radiotracers for PET studies of the norepinephrine transporter. Nucl Med Biol. 1997; 24: 707-711.

25. Kirjavainen AK, Forsback S, López-Picón FR, et al. 18F-labeled norepinephrine transporter tracer [¹⁸F]NS12137:radiosynthesis and preclinical evaluation. Nucl Med Biol. 2018; 56: 39-46.

26. Peters D, Eriksen BL, Nielsen EØ, Scheel-Krüger J, Olsen GM. Novel 8-azabicyclo[3.2.1]octane derivatives and their use as monoamine neurotransmitter reuptake inhibitors. WO 2004/113334 A1; 2004.

27. Vase KH, Peters D, Nielsen EØ, Alstrup AKO, Bender D. [¹¹C]NS8880, a promising PET radiotracer targeting the norepinephrine transporter. Nucl Med Biol 2014: 41; 758-64.

28. DanPET AB. On file. Methods used for generation of data described in: Andreasen JT, Redrobe JP, Nielsen EØ, Christensen JK, Olsen GM, Peters D. A combined α7 nicotinic acetylcholine receptor agonist and monoamine reuptake inhibitor, NS9775, represents a novel profile with potential benefits in emotional and cognitive disturbances. Neuropharmacology. 2013; 73: 183-191.

29. Sanders JD, Happe HK, Bylund DB, Murrin LC. Development of the norepinephrine transporter in the rat CNS. NeuroScience. 2005; 130: 107-117.

30. Moriguchi S, Kimura Y, Masanori I et al. PET quantification of the norepinephrine transporter in human brain with (S,S)-18F-FMeNER-D2. J Nucl Med 2017; 58: 1140–1145.

31. German DC, Walker BS, Manaye K, Smith WK, Woodward DJ, North AJ. The human locus coeruleus: computer reconstruction of cellular distribution. J Neurosci. 1988; 8: 1776-1788.

32. Theofilas P, Ehrenberg AJ, Dunlop S, et al. Locus coeruleus volume and cell population changes during Alzheimer's disease progression: A stereological study in human postmortem brains with potential implication for early-stage biomarker discovery. Alzheimers Dement. 2017; 13: 236-246.

33. Lebow MA, Chen A. Overshadowed by the amygdala: the bed nucleus of the stria terminalis emerges as key to psychiatric disorders. Mol Psychiatry. 2016; 21: 450-463.

34. Avery SN, Clauss JA, Blackford JU. The human BNST: functional role in anxiety and addiction. Neuropsychopharmacology. 2016; 41: 126-141.

35. Briard E, Zoghbi SS, Siméon FG, et al. Single-step high-yield radiosynthesis and evaluation of a sensitive ¹⁸F-labeled ligand for imaging brain peripheral benzodiazepine receptors with PET. J Med Chem. 2009 52: 688-699.

36. Siméon FG, Brown AK, Zoghbi SS, Patterson VM, Innis RB, Pike VW. Synthesis and simple ¹⁸F-labeling of 3-fluoro-5-(2-(2-(fluoromethyl)thiazol-4-yl)ethynyl)benzonitrile as a high affinity radioligand for imaging monkey brain metabotropic glutamate subtype-5 receptors with positron emission tomography. J Med Chem. 2007; 50: 3256-3266.

37. Tipre DN, Zoghbi SS, Liow JS, et al. PET imaging of brain 5-HT1A receptors in rat *in vivo* with ¹⁸F-FCWAY and improvement by successful inhibition of radioligand defluorination with miconazole. J Nucl Med. 2006; 47: 345-353.